

Accepted Article

Title: Graphene Enhanced Photo-Electrochemical Water Splitting by Diminishing Pt/p-Si Photocathode Interfacial Barrier

Authors: Xiaodong Zhu, Xue Yu, Jiangli Li, Hao Li, Shuai Wang, Yuchen Xu, Yanqing Ma, and Lei Ma

This manuscript has been accepted after peer review and appears as an Accepted Article online prior to editing, proofing, and formal publication of the final Version of Record (VoR). The VoR will be published online in Early View as soon as possible and may be different to this Accepted Article as a result of editing. Readers should obtain the VoR from the journal website shown below when it is published to ensure accuracy of information. The authors are responsible for the content of this Accepted Article.

To be cited as: *ChemPhotoChem* **2023**, e202200272

Link to VoR: <https://doi.org/10.1002/cptc.202200272>

Graphene Enhanced Photo-Electrochemical Water Splitting by Diminishing Pt/*p*-Si Photocathode Interfacial Barrier

Xiaodong Zhu^[a], Xue Yu^[a], Jiangli Li^[a], Hao Li^[a], Shuai Wang^[a], Yuchen Xu^[a],

Yanqing Ma^{*[a],[b]} and Lei Ma^{*[a]}

[a] X. Zhu, X. Yu, J. Li, H. Li, S. Wang, Y. Xu, Y. Ma, L. Ma
Tianjin International Center for Nanoparticles and Nanosystems, Tianjin University, Tianjin 300072, P. R. China
Email: mayanqing@tju.edu.cn, E-mail: lei.ma@tju.edu.cn

[b] Y. Ma
School of Precision Instrument & Opto-Electronics Engineering, Tianjin University, Tianjin 300072, P. R. China

Supporting information for this article is given via a link at the end of the document.

Abstract: Converting solar energy into hydrogen by photo-electrochemical cells is believed to be one of the most promising strategies to acquire clean energy. However, one barricade for further improving the performance of photocathode system is the flattening of Schottky barrier formed at the interface between the *p*-type photo-absorber and metal co-catalyst (e.g. Pt/*p*-Si) due to the mismatch of their Fermi levels. Here, we present a facile way of making photocathodes by transferring high quality CVD graphene onto *p*-type Si as a buffer layer, which can effectively diminish the Pt/*p*-Si interfacial barrier and promoting charge separation efficiency, hence, improve photo-electrochemical performance of such a device for hydrogen generation. The measured photocurrent density is 3.9 times higher than that were achieved without graphene buffer. This approach offers a novel route to decrease the Pt/*p*-Si interfacial barrier for developing future highly efficient solar conversion systems. It can easily be extended to many other photocathode systems.

Introduction

The rapid consumption of fossil fuels triggers enormous anxieties on the sustainability of high speed development of human society in near future, whereas, it motivated an active pursuit for clean and sustainable energy resources in past decades. Solar energy has been considered as one of the most promising substitution among a variety of candidates due to its eco-friendly, low-cost accessibility and inexhaustibility in nature^[1].

Except photovoltaic (PV) panels, which yet has been developed and commercialized for years, conversion of sunlight into hydrogen (H₂) by electrolysis provides an effective alternative for energy storage and distribution with no cyclic fluctuations comparing to the PV grid^[1a]. Owing to the abundant choices of materials, high efficiency and low extent of complexity^[2], PEC systems based solar-driven water electrolysis become one of the most potential routes for realizing future cheap, durable and environmental friendly approaches in solar-driven hydrogen production. Commercially available silicon (Si) based materials have been the feasible electrode choices of PEC due to their easy-accessibility, reasonable light conversion efficiency and appropriate band gap, which are the decisive factors for obtaining the best visible light absorption and optimal external bias^[3]. The *p*-doped and *n*-doped Si are normally chosen as cathode and anode materials, respectively, due to their specific band bending directions in water electrolyte^[2a, 4].

In order to realize high solar-to-hydrogen conversion efficiency for Si based devices, two major techniques have been employed: 1) maximizing photo-absorption through surface/interface engineering and 2) overcoming sluggish water reduction/oxidation kinetics of silicon by loading surface co-catalyst^[5]. Surface texturing, such as forming nano-pyramid^[6], nano-groove and nanowire^[7] *et al.*, has been intensively explored, which is an approved effective approach to reduce the surface light reflectivity and furthermore improve the light harvesting efficiency. However, they often will unavoidably create undesirable charge trap centers on electrode and in turn largely increase the photo-excited charge recombination also lead to the so-called fermi level pinning, and consequently deteriorate the light-current efficiency. Thus, extra surface passivation process (TiO₂, Al₂O₃, Ni, etc) often has to be introduced to stabilize and protect Si surface for resolving above issues including photo-corrosion^[8]. Usually, the key of applying the co-catalyst loading method is to minimize the cost through lower the dose of noble metal catalyst loading and avoiding creating high Schottky barriers via interface/surface engineering^[8c], which requires that the work function and morphology of the co-catalyst layer must be carefully tuned to match the semiconductor substrate.

Therefore, in the past decades, numerous experiments have been conducted to try to find the best materials and approaches for Si based PEC system both for surface passivation as well as the co-catalysis with positive synergistic effects. Yu *et al.* fabricated a SrTiO₃ protected Si photocathode with lithography patterned Pt/Ti nano-spheres coating^[9]. Later, Li *et al.*^[10] and Chung *et al.*^[11] achieved high photo-electrochemical H₂ evolution on planar Si photocathodes through Ni/Fe co-doped In₂S₃ nano-sheet arrays and three-dimensionally patterned Ag-Pt alloy catalyst, respectively. Moreover, A. Smith *et al.* employed RF magnetron to grow ultra-thin Ni/Pt films which effectively realized the minimization of light transmission loss.^[8c] Apparently, an ideal candidate should be passivation effective, transparent as well as low cost. However, these approaches often involve much more complicated material synthesis and fabrication process.

As a rising star new material, graphene owns all needed features what are discussed above. It is atomically thin, chemical inert with extremely high thermal and electric conductivity^[12], transparent^[13], and very mild problem of the Schottky barrier by interfacing with noble metal^[8c, 14]. Therefore, it potentially can be used as a great candidate for such kind of

applications. By applying graphene can prohibit the direct contact between Pt and Si, the main function is to eliminate the possible fermi level-pinning effect. In addition, due to its chemical inertness, it would also improve the interface stability of graphene/p-Si junction. So far, high quality graphene have rarely been employed as photo-catalysis for PEC systems yet. Although there have been some attempts of using reduced-graphene oxide for realizing the similar goal^[15], however, it could neither fully take the privilege of the intrinsic electric properties of graphene due to its low quality nor the high transparency of graphene layer caused by their highly wrapped and overlapped flakes^[16].

Here, we developed a catalyst composed by high quality CVD graphene p-Si surfaces with an ultrathin Pt layer on top^[5c], which demonstrates 3.9 folds enhanced hydrogen evolution reaction (HER) efficiency than that without graphene layer. The device fabrication and measuring procedures are illustrated as in Fig. 1. The core of this work is to design a sandwiching system to apply graphene as an effective passivation layer for silicon surface and also presumably hire it to serve as a supporting conductive layer to promote the catalytic process of Pt nanoparticles by exploiting the extraordinary electric conductivity of graphene. Comparing to other passivation layers, graphene is so unique by combining high transparency, high conductivity, effective passivation with ultrathin thickness.

More importantly, due to the feasibility and low cost of graphene transfer onto a wide variety of substrates, this technique can be easily coupled with many other non-Si based photosystems as an extra way to developing stable and advanced PEC cells which paves the road for their industrial applications.

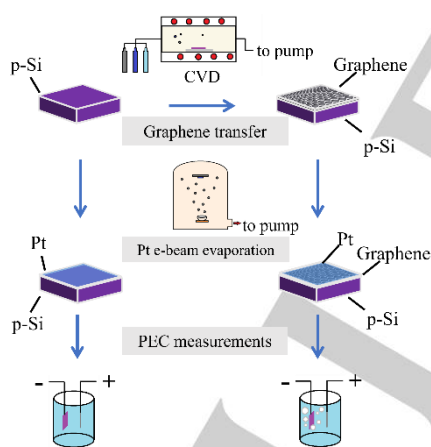


Figure 1. The schematic fabrication process of Pt/p-Si photocathodes with and without graphene buffer.

Results and Discussion

Characterizations of CVD Grown Graphene

It is of great importance to check the quality of the transferred graphene. A series of characterizations have been conducted to evaluate the uniformity, thickness, conductivity and doping property of the transferred CVD graphene as shown in Fig. 2. The SEM image indicates its highly homogenous morphology and thickness (Fig. 2a). The few bright spot seen in the image may come from the carbon nucleation during the growth. A much higher contrasted image was only seen near the

edge of the film (Fig. S1) demonstrating the film's uniformity in large scale.

The Raman spectrum of transferred graphene on Si (Fig. 2b) revealed three major bands, D, G and 2D at 1350 cm^{-1} , 1580 cm^{-1} and 2700 cm^{-1} , respectively^[17]. The narrow FWHM ($\sim 34\text{ cm}^{-1}$) of the 2D band, high I_{2D}/I_G (~ 4) ratio, and low I_D/I_G ratio demonstrate that they are high quality single layer dominated graphene films with low defects density^[18].

Linearity of I-V (Fig. 2c) curve indicates the low Ohmic contact resistance of the device^[19]. More importantly, the shift of the charge neutral point (CNP) (Fig. 2d) indicates its slightly p-type doping^[19b], which can be attributed to the absorption of O_2 , H_2O and other adsorbates from air.^[20] Moreover, the interaction of these charge traps and movable charges with graphene carriers leads to the observed hysteresis effect^[20-21]. UV-visible spectrum measurements of the transferred graphene samples demonstrate its high transmission rate as shown in Fig. S2. Thus, we believe the quality of our graphene is high enough to separate Pt from contacting with Si.

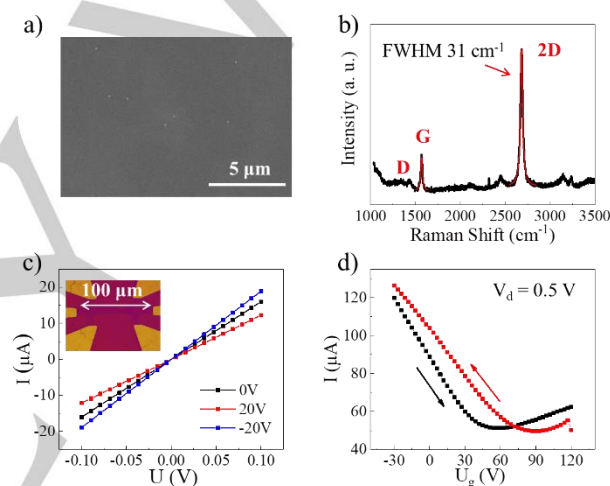


Figure 2. The a) SEM characterization, b) Raman spectrum of CVD grown graphene transferred onto Si substrates and c) I-V d) transfer curve measurements of graphene channel fabricated on SiO_2/Si back-gated device.

Photo-Electrical Properties of Pt/graphene/p-Si Junction

Photo-electrochemical measurements were firstly conducted on the graphene/p-Si junctions. As shown in Fig. 3a, the LSV were measured on the graphene/p-Si photocathodes in $0.5\text{ M Na}_2\text{SO}_4$ (pH 7) under AM 1.5G 100 mW cm^{-2} illumination. It is noticeable that the blank Si barely shows any reactivity (-0.17 mA cm^{-2}), as illustrated by the blue line in Fig. 3a. However, after introducing the graphene buffer, a significant photocurrent improvement (-1.23 mA cm^{-2}) was obtained as demonstrated by the red line in Fig. 3a. Meanwhile, a more positive onset potential (-0.065 V) was achieved which possibly due to the p-Si band edge bending downwards for the much higher graphene E_f ($\approx -4.5\text{ eV}$ vs. E_{vac} ^[14a]), therefore largely facilitates electron transfer towards the electrolyte.

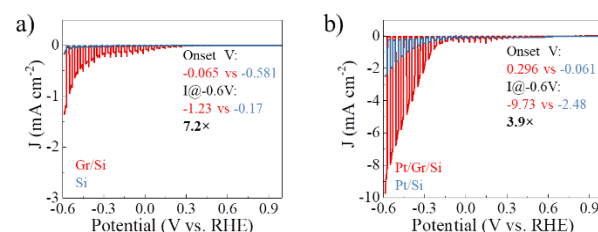


Figure 3. Photocurrent density-potential (I-V) curves of graphene buffered (Red) and non-buffered (Blue) a) *p*-Si and b) Pt/*p*-Si photocathodes under AM 1.5G (100 mW·cm⁻²) in 0.5 M Na₂SO₄ solution. Onset potential are defined at 0.1 mA·cm⁻².

This trend is also displayed in the Mott-Schottky plots as shown in Fig. 4a-b, as the E_{fb} positioned much higher comparing the samples with and without graphene (-0.35V vs. -0.45 V). Meanwhile, the highly repeatable hill-like difference is mainly due to the interfacial Schottky barrier caused by direct contact between Pt and Si. One key rule to be followed for developing hydrogen evolution reaction (HER) catalysts is the so-called volcano curve, which reflects the relation between HER catalytic effectiveness and chemisorption energy of hydrogen on catalyst surfaces^[22]. Platinum (Pt) falls near the apex of this volcano and has long been recognized as the state-of-the-art electro-catalyst in water splitting, especially HER for its proper chemisorption energy of hydrogen (neither too strongly nor too weakly)^[5a]. Much effort have been devoted to either minimizing the mass loading of Pt or seeking non-Pt earth-abundant replacements with suitable hydrogen bonding strength^[5a, 23]. In our case, a 2nm thick Pt layer was deposited onto the substrates by e-beam evaporation, which balances the acquiring of high mass activity and minimization usage of Pt^[6c]. Moreover, such thin layer of Pt is almost 100% transparent (Fig. S3) across the UV-vis spectrum which allows the maximum usage of light.

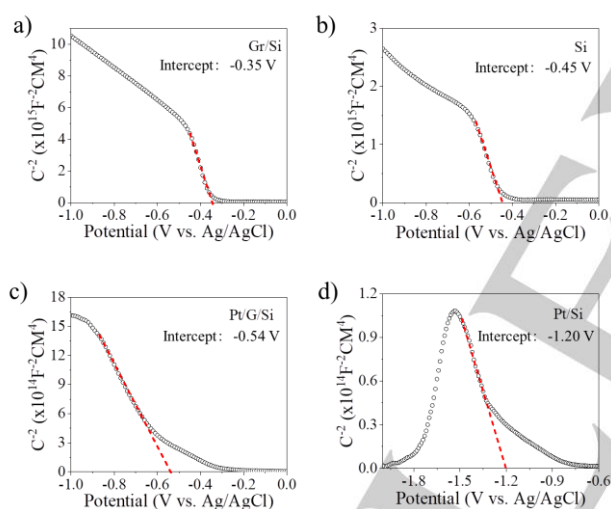


Figure 4. Mott-Schottky plots of a) graphene/Si, b) bare Si, c) Pt/graphene/Si and d) Pt/Si photocathodes in 0.5 M Na₂SO₄ solution with light avoided conditions.

However, the key issue of combing Pt with *p*-Si photocathode is to flatten the Schottky barrier formed due to the fermi level miss-alignment of *p*-Si ($E_f \approx -5.1\text{eV}$ vs. E_{vac}) and Pt ($E_f \approx -5.6\text{eV}$ vs. E_{vac})^[8c] since the upwards bending band edge will hinder the electron transfer from Si to adsorbed H atoms and results in a small open circuit voltage (V_{oc})^[9]. Therefore, low work function metals, e.g. Ti^[9], together with wide band gap semiconductor (TiO₂^[14b]) and insulators (SrTiO₃^[9], SiO₂^[24], Al₂O₃^[8c]) has been sandwiched between the Si and Pt^[9, 24]. This implies the great potential of graphene serving as an ideal layer between the *p*-Si substrate and Pt metal to flatten the Si/Pt Schottky junction due to its high conductivity, high transparency and suitable work function ($E_f \approx -4.5\text{eV}$ vs. E_{vac}) (Fig. 5).^[14a]

Fig. 3b shows the current density (I) - electrode potential (V) curves for H₂ generation on the fabricated Pt/graphene/*p*-Si photocathodes in 0.5 M Na₂SO₄ solution under simulated AM 1.5G 100 mW·cm⁻¹ illumination. Comparing with the previous results without Pt catalyst, much higher photo-current densities were obtained on samples after loading Pt catalyst as expected. A notable (≈ 3.9 times) increased current density was observed between Pt/*p*-Si photocathodes with (-9.73 mA·cm⁻²) and without graphene (-2.48 mA·cm⁻²) as buffer layer at -0.6 V. Meanwhile, the measured onset potential (defined as the potential at a photo-current of 0.1 mA·cm⁻²) also exhibits a shift from -0.061 to 0.296 V indicates the improvement of V_{oc} .

In comparison, Ku *et al.* achieved -37.5 mA/cm² at -0.6 V with Gr/Pyramid-Si system^[25]. Under the same biased voltage, Lim *et al.* obtained -35 mA/cm² at -0.6 V with 3D-AgPt/*p*-Si structure^[11]; Meng *et al.* obtained ≈ 4 mA/cm² with Fe:In₂S₃/Si and ≈ 10 mA/cm² with Ni:In₂S₃/Si^[10]; Berglund *et al.* achieved ≈ 18 mA/cm² with Pt/W₂C/*p*-Si^[26]; the Talin group achieved ≈ 13 mA/cm² with Pt/Ti/Si^[24].

The rather poor performance in our case as shown in Fig. 3 is mainly due to the planner structure of Si, we believe it could be largely improved by a surface reconfigurations or texturing for enlarging its effective surface area.

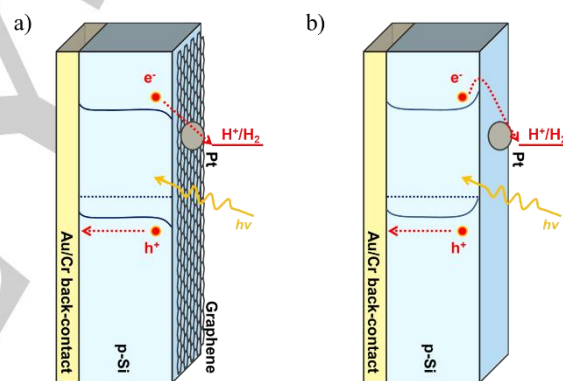


Figure 5. The schematic diagram of graphene buffer flattening the Pt/*p*-Si interfacial barrier.

The improvement of current-density could be attributed to the formation of Pt/graphene/Si hetero-junction, which decreases the Pt/*p*-Si barrier, therefore facilitates the photo-generated electron transmission towards the Pt, in turn, it results in a higher charge separation efficiency of adsorbed H atoms with light illumination. A positive potential onset shift at graphene/*p*-Si junction photocathode compare to that of the pristine Si may be caused by the shift of the photo electrode flat-band potential (E_{fb}). E_{fb} can be determined from linearly extrapolating the Mott-Schottky curve. As shown in Fig. 4c-d, the Pt/graphene/*p*-Si junction exhibits a more positive E_{fb} than that of pristine *p*-Si indicating the decrease of production potential due to the existence of the graphene layer, which is consistent with the positive onset potential shift.

In addition, as clearly shown in the measurements of electrochemical impedance spectroscopy (EIS) in Fig.6, the sample with graphene buffered (Red) shows much smaller semicircle comparing to the non-buffered one (Blue). Similar trend was observed under light condition as shown in Fig. S4.

The semicircle in the high frequency range represents the charge transfer loss, its short radius implies a small charge transfer resistance. This advantage was also observed while comparing to traditional TiO₂ buffered Pt/*p*-Si samples as shown in Fig. S5.

At last, a stability test has been applied on graphene buffered Pt/Si sample and we have obtained a generally stable trend in photocurrent density within the time-length of 2 hours as shown in Fig. S6.

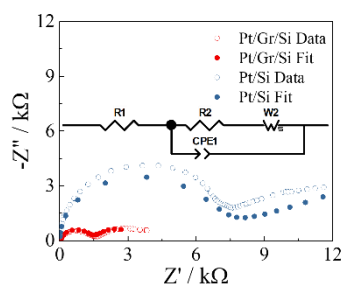


Figure 6. EIS plots graphene buffered (Red) and of graphene buffered and non-buffered a) *p*-Si and b) Pt/*p*-Si photocathodes in 0.5 M Na₂SO₄ solution with light avoided conditions. Inset: the fitting circuit.

Photo-Electrical Properties of Pt/graphene/*p*-Si3D Junction

Similar experiments have also been conducted on (three dimensional) 3D textured Si surfaces. Technically, such texturing (pyramid structures^[25, 27], nano-porous^[28], micro-arrays^[7a], etc) can significantly expand the surface area of Si for better light absorption. In this work, a simple one-step etching process was adopted to fabricate textured Si surface (Si3D) as shown in Fig. S7a. Raman spectra of the transferred graphene on this surface have been shown in Fig. S7b. The narrow FWHM of 2D band and low D band level evidence the authenticity of transferred graphene.

Again, e-beam evaporation process was conducted to guarantee the equality amount of Pt deposition on both 3D and planar Si surfaces to a great accuracy. Interesting, we do not observe the expected amount of improvement in comparing the photo-current density of Pt/Si3D (blue lines in Fig. S7c) and Pt/Si planar samples (blue lines in Fig. 3b) due to the largely incremental surface area. In addition, it was noticeable that the enhancement by the graphene buffer (red lines in Fig. S7c) was low (≈ 1.8 times) comparing to the planar Si counterpart (≈ 3.9 times) (red lines in Fig. 3b). Similar to the previous planar Si results, M-S measurement displays a higher E_b (≈ 0.25 V) of Pt/graphene/Si3D than Pt/Si3D, as shown in Fig. S8. Typically, roughing the Si substrate surface leads to an enhancing of photo-current due to larger surface area, however, in this case similar effect was not observed, it can be attributed much less contact between graphene and the textured silicon surface which further resulted very weak interact among the silicon with Pt layer. Subsequently, effective HER catalysis only occurs at the very little amount of Pt/graphene/*p*-Si tri-layer stacking regions. This could be the major reason that we have not observed a significantly boost on photo-current density while comparing 3D to planar Si substrate although the former has an obvious higher surface area.

In short, we have shown the universal ability of graphene as a buffer to couple with different *p*-Si morphological surfaces,

which is critical for integrating with main stream PEC technology. This work also suggests that flattening the Schottky barrier at metal/*p*-Si interface with graphene could provide an additional tuning knob in improving charge-separation efficiency of devices.

Conclusion

In summary, by taking advantages of graphene induced charge transport facilitation and Pt/*p*-Si Schottky barrier flattening, we have developed Pt/graphene/Si junction photocathodes for efficient PEC hydrogen evolution reaction through transferring high quality single layer CVD graphene on to *p*-Si surfaces and in further clarifies the charge transfer mechanism at the Pt/graphene/*p*-Si interfaces. These demonstrate that graphene layers on 2D planar *p*-Si surfaces exhibited excellent HER effects. It illustrates that introducing of graphene into traditional Si PEC cells is an extra and highly compatible approach to improve the efficiency of *p*-Si based photo-water splitting systems which can further benefit the PEC solar energy conversion industry.

Experimental Section

Growth and Characterization of Graphene High quality graphene layer was synthesized on copper foil (purchased from Haisi Lab, Beijing, China, 99%, 25 μm) by ambient pressure vapor deposition (APCVD). The copper foils were cut into 8 mm \times 8 mm squares and ultrasonically rinsed by acetone, ethanol and deionized water 15 min each sequentially. Then, the cleaned copper foils were placed on a corundum boat inside a horizontal quartz tubing (1200 mm \times Φ 60 mm) in a CVD furnace. The tube was pumped down below 0.1Pa and then constantly flooded with 1atm mixture of H₂ and Ar (1:4 ratio). Subsequently, the furnace was heated up to 1050 $^{\circ}\text{C}$ within 80 min and kept for 40 min. Then, methane (CH₄) was introduced as the carbon source with a flow rate of 1sccm. After 13 min growth, the furnace was cooled down to 400 $^{\circ}\text{C}$ linearly in 40 min and then cooled down to room temperature.

The surface morphology of graphene films was characterized by a Hitachi SU3500 scanning electron microscope (SEM) with an accelerating voltage of 5 kV. The thickness and quality of graphene films was characterized by a Raman spectrometer with 1 μm diameter focal spot and 40 mW, 532 nm laser excitation. UV-Vis (DRS, Hitachi U-3900) spectra were acquired to analyze the light transmission.

Graphene back-gated FET devices were fabricated on SiO₂/Si substrate to evaluate its electronic properties. UV-lithography and e-beam evaporation were used to form Cr/Au electrodes (30/15 nm) and graphene channel (100 μm \times 10 μm) for the metal electrode and graphene channel fabrication. Reactive ion etching (RIE) etching was performed (RF power 25 W, O₂ 30 sccm, 25 s) to remove the unwanted graphene other than the channel. Then the electronic properties of graphene were evaluated using a probe-station.

Fabrication of Pt/Graphene/*p*-Si Photocathode A 525 \pm 10 μm thick, *p*-type, (100) Si wafer (resistivity of 0.1-0.5 $\Omega\cdot\text{cm}$) (KJ Group, Hefei, China) was diced into 9 mm \times 12 mm chips and ultrasonically rinsed using acetone, iso-propanol and deionized-water sequentially. Each sample was then treated by HF (2%) solution 60 s to remove the surface oxide layer. Afterwards, Au/Cr (15/30 nm) backside electrodes were deposited by using an e-beam evaporator (DZS500, SKY Technology Development Co., Ltd, China). The detailed graphene transfer process is described in details in supporting information (SI). The same e-beam evaporation chamber was also used for the Pt catalyst deposition under 6.6 \times 10⁻⁴ Pa with a rate of 0.02 $\text{\AA}\cdot\text{s}^{-1}$. The deposition process was

monitored by an in situ quartz crystal microbalance (QCM) and the thickness of Pt was carefully controlled to be ~ 2 nm with low deposition rate and calibrated by using Atomic Force Microscopy^[5c].

Photo-Electrochemical Measurements The back-side of the sample was completely sealed to avoid contacting electrolyte. The front-side of the sample was partially sealed with an opening of 5×6 mm² to expose to electrolyte. The size of graphene transferred is determined by the size of the copper foil, and we have made sure the PEC measurement window was smaller than the film of graphene. A three-electrode cell was used to measure the reaction current where the p-Si based photocathode, Pt wire and Ag/AgCl (sat. KCl solution) were used as working electrode, counter electrode and reference electrode, respectively. 0.5 M Na₂SO₄ solution with pH of 7 was chosen as electrolyte. Xenon lamp (CEL-HXF300, Au Light, China) with AM 1.5 G optical filter were used to mimic sun light with a calibrated power of 100 mW · cm⁻². Linear sweep voltammetry (LSV) curves were collected by measuring the current density ranges from 0.4 to -1.2 V versus Ag/AgCl with a scan rate of 20 mV · s⁻¹ using a CHI 760E electrochemical workstation (CH Instruments Inc, Shanghai, China) without IR compensation. Electrochemical impedance spectrum (EIS) was recorded within the range of 0.1 Hz to 100 kHz with no light exposure^[29]. Meanwhile, Mott-Schottky measurements were performed from -0.6 to 0.6 V with an incremental voltage of 0.025 V/step.

Acknowledgements

This work was financially supported by the National Natural Science Foundation of China (No. 11774255), the National Key R&D Program of China (2020YFC2004602) and Postdoctoral Research Foundation of China (No. 2019M661023).

Keywords: graphene, photocathode, interfacial barrier, hydrogen evolution reaction

- [1] a) J. H. Kim, D. Hansora, P. Sharma, J.-W. Jang, J. S. Lee, *Chem. Soc. Rev.* **2019**, *48*, 1908-1971; b) K. Sun, S. Shen, Y. Liang, P. E. Burrows, S. S. Mao, D. Wang, *Chem. Rev.* **2014**, *114*, 8662-8719; c) S. J. A. Moniz, S. A. Shevlin, D. J. Martin, Z.-X. Guo, J. Tang, *Energ. Environ. Sci.* **2015**, *8*, 731-759.
- [2] a) T. Yao, X. An, H. Han, J. Q. Chen, C. Li, *Adv. Energy Mater.* **2018**, *8*, 1800210; b) C. Ding, J. Shi, Z. Wang, C. Li, *ACS Catal.* **2017**, *7*, 675-688.
- [3] Z. Luo, T. Wang, J. Gong, *Chem. Soc. Rev.* **2019**, *48*, 2158-2181.
- [4] J. Cen, Q. Wu, M. Liu, A. Orlov, *Green Energy Environ.* **2017**, *2*, 100-111.
- [5] a) I. Roger, M. A. Shipman, M. D. Symes, *Nat. Rev. Chem.* **2017**, *1*, 0003; b) L. Liao, Q. Zhang, Z. Su, Z. Zhao, Y. Wang, Y. Li, X. Lu, D. Wei, G. Feng, Q. Yu, X. Cai, J. Zhao, Z. Ren, H. Fang, F. Robles-Hernandez, S. Baldelli, J. Bao, *Nat. Nanotechnol.* **2013**, *9*, 69; c) Y. Wang, X. Yu, G. Liu, X. Zhu, R. Xu, M. Ji, Y. Ma, L. Ma, *Adv. Sustainable Syst.* **2019**, *3*, 1900026.
- [6] a) X. Cheng, H. Shen, W. Dong, F. Zheng, L. Fang, X. Su, M. Shen, *Adv. Mater. Interfaces* **2016**, *3*, 1600485; b) J. Yang, K. Walczak, E. Anzenberg, F. M. Toma, G. Yuan, J. Beeman, A. Schwartzberg, Y. Lin, M. Hettick, A. Javey, J. W. Ager, J. Yano, H. Frei, I. D. Sharp, *J. Am. Chem. Soc.* **2014**, *136*, 6191-6194.
- [7] a) S. W. Boettcher, E. L. Warren, M. C. Putnam, E. A. Santori, D. Turner-Evans, M. D. Kelzenberg, M. G. Walter, J. R. McKone, B. S. Brunschwig, H. A. Atwater, N. S. Lewis, *J. Am. Chem. Soc.* **2011**, *133*, 1216-1219; b) T. R. Hellstern, A. C. Nielander, P. Chakhranont, L. A. King, J. J. Willis, S. Xu, C. MacIsaac, C. Hahn, S. F. Bent, F. B. Prinz, T. F. Jaramillo, *ACS Appl. Nano Mater.* **2019**, *2*, 6-11.
- [8] a) M. R. Shaner, S. Hu, K. Sun, N. S. Lewis, *Energ. Environ. Sci.* **2015**, *8*, 203-207; b) M. J. Kenney, M. Gong, Y. Li, J. Z. Wu, J. Feng, M. Lanza, H. Dai, *Science* **2013**, *342*, 836-840; c) I. A. Digdaya, G. W. P. Adhyaksa, B. J. Trześniewski, E. C. Garnett, W. A. Smith, *Nat. Commun.* **2017**, *8*, 15968; d) Y. W. Chen, J. D. Prange, S. Dühnen, Y. Park, M. Gunji, C. E. D. Chidsey, P. C. McIntyre, *Nat. Mater.* **2011**, *10*, 539-544.
- [9] L. Ji, M. D. McDaniel, S. Wang, A. B. Posadas, X. Li, H. Huang, J. C. Lee, A. A. Demkov, A. J. Bard, J. G. Ekerdt, E. T. Yu, *Nat. Nanotechnol.* **2014**, *10*, 84.
- [10] L. Meng, J. He, W. Tian, M. Wang, R. Long, L. Li, *Adv. Energy Mater.* **2019**, *9*, 1902135.
- [11] S. Y. Lim, K. Ha, H. Ha, S. Y. Lee, M. S. Jang, M. Choi, T. D. Chung, *Phys. Chem. Chem. Phys.* **2019**, *21*, 4184-4192.
- [12] a) S. V. Morozov, K. S. Novoselov, M. I. Katsnelson, F. Schedin, D. C. Elias, J. A. Jaszczak, A. K. Geim, *Phys. Rev. Lett.* **2008**, *100*, 016602; b) A. H. C. Neto, *Phys. Status Solidi* **2010**, *244*, 4106-4111; c) C. Berger, E. H. Conrad, W. A. de Heer, *arXiv preprint arXiv:1704.00374* **2017**; d) J. Baringhaus, M. Ruan, F. Edler, A. Tejada, M. Sicot, A. Taleb-Ibrahimi, A.-P. Li, Z. Jiang, E. H. Conrad, C. Berger, *Nature* **2014**, *506*, 349.
- [13] R. R. Nair, P. Blake, A. N. Grigorenko, K. S. Novoselov, T. J. Booth, T. Stauber, N. M. Peres, A. K. Geim, *Science* **2008**, *320*, 1308-1308.
- [14] a) G. Giovannetti, P. A. Khomyakov, G. Brocks, V. M. Karpan, J. van den Brink, P. J. Kelly, *Phys. Rev. Lett.* **2008**, *101*, 026803; b) C. Ros, T. Andreu, M. D. Hernández-Alonso, G. Penelas-Pérez, J. Arbiol, J. R. Morante, *ACS Appl. Mater. Interfaces* **2017**, *9*, 17932-17941.
- [15] a) Y. Ghayeb, M. M. Momeni, M. Menati, *J. Mater. Sci.: Mater. Electron.* **2017**, *28*, 7650-7659; b) B. Koo, S. Byun, S.-W. Nam, S.-Y. Moon, S. Kim, J. Y. Park, B. T. Ahn, B. Shin, *Adv. Funct. Mater.* **2018**, *28*; c) A. Iwase, Y. H. Ng, R. Amal, A. Kudo, *J. Mater. Chem. A* **2015**, *3*, 8566-8570.
- [16] a) A. Mondal, A. Prabhakaran, S. Gupta, V. R. Subramanian, *ACS Omega* **2021**, *6*, 8734-8743; b) M. Y. A. Rahman, *J. Mater. Sci.: Mater. Electron.* **2021**, *32*, 23690-23719.
- [17] F. Tuinstra, J. L. Koenig, *J. Chem. Phys.* **1970**, *53*, 1126-1130.
- [18] a) Z. Ni, Y. Wang, T. Yu, Z. Shen, *Nano Res.* **2008**, *1*, 273-291; b) A. C. Ferrari, J. C. Meyer, V. Scardaci, C. Casiraghi, M. Lazzeri, F. Mauri, S. Piscanec, D. Jiang, K. S. Novoselov, S. Roth, *Phys. Rev. Lett.* **2006**, *97*, 187401; c) S. Zhengzong, Y. Zheng, Y. Jun, B. Elvira, Z. Yu, J. M. Tour, *Nature* **2010**, *468*, 549-552.
- [19] a) X. Yan, Y. Wu, R. Li, C. Shi, R. Moro, Y. Ma, L. Ma, *ACS Omega* **2019**, *4*, 14179-14187; b) L. Zhao, Y. Wang, X. Zhu, P. Ji, K. Zhang, X. Yu, C. Shi, R. Li, Y. Ma, L. Ma, *Mater. Res. Express* **2019**, *6*, 105604.
- [20] A. Veligura, P. J. Zomer, I. J. Vera-Marun, C. Józsa, P. I. Gordiichuk, B. J. v. Wees, *J. Appl. Phys.* **2011**, *110*, 113708.
- [21] H. Wang, Y. Wu, C. Cong, J. Shang, T. Yu, *ACS Nano* **2010**, *4*, 7221-7228.
- [22] S. Trasatti, *J. Electroanal. Chem. Interfacial Electrochem.* **1972**, *39*, 163-184.
- [23] J. Cai, R. Javed, D. Ye, H. Zhao, J. Zhang, *J. Mater. Chem. A* **2020**, *8*, 22467-22487.
- [24] D. V. Esposito, I. Levin, T. P. Moffat, A. A. Talin, *Nat. Mater.* **2013**, *12*, 562.
- [25] C.-K. Ku, P.-H. Wu, C.-C. Chung, C.-C. Chen, K.-J. Tsai, H.-M. Chen, Y.-C. Chang, C.-H. Chuang, C.-Y. Wei, C.-Y. Wen, T.-Y. Lin, H.-L. Chen, Y.-S. Wang, Z.-Y. Lee, J.-R. Chang, C.-W. Luo, D.-Y. Wang, B. J. Hwang, C.-W. Chen, *Adv. Energy Mater.* **2019**, *9*, 1901022.
- [26] S. P. Berglund, H. He, W. D. Chemelewski, H. Celio, A. Dolocan, C. B. Mullins, *J. Am. Chem. Soc.* **2014**, *136*, 1535-1544.
- [27] F. Chen, Q. Zhu, Y. Wang, W. Cui, X. Su, Y. Li, *ACS Appl. Mater. Interfaces* **2016**, *8*, 31025-31031.
- [28] J. Oh, T. G. Deutsch, H.-C. Yuan, H. M. Branz, *Energ. Environ. Sci.* **2011**, *4*, 1690-1694.
- [29] Y. Shi, Z. Lu, L. Guo, C. Yan, *Int. J. Hydrogen Energy* **2017**, *42*, 26183-26191.

Table of Content

By transferring high quality CVD graphene onto p-type Si as a buffer layer, the Pt/p-Si interfacial barrier can effectively be diminished and thus promote charge separation efficiency. This approach leads to an improved photo-electrochemical performance for hydrogen generation which offers a novel and easily transferable route for developing future high efficient solar conversion systems.

